Physics and Imaging in Radiation Oncology 20 (2021) 11–16

Contents lists available at ScienceDirect

Physics and Imaging in Radiation Oncology

journal homepage: www.sciencedirect.com/journal/physics-and-imaging-in-radiation-oncology

In-vivo X-ray dark-field computed tomography for the detection of radiation-induced lung damage in mice

Rico Burkhardt [a,b,c,1], Thomas Gora [a,1], Alexander A. Fingerle [d], Andreas P. Sauter [d], Felix Meurer [d], Florian T. Gassert [d], Sophie Dobiasch [a,b], Daniela Schilling [a,b], Annette Feuchtinger [g], Axel K. Walch [g], Gabriele Multhoff [a,b,h], Julia Herzen [c,e,f], Peter B. Noël [d], Ernst J. Rummeny [d], Stephanie E. Combs [a,b,i], Thomas E. Schmid [a,b], Franz Pfeiffer [c,d,e,f], Jan J. Wilkens [a,c,e,*]

[a] Department of Radiation Oncology, Technical University of Munich, School of Medicine and Klinikum rechts der Isar, Munich, Germany
[b] Institute of Radiation Medicine (IRM), Helmholtz Zentrum München, Neuherberg, Germany
[c] Physics Department, Technical University of Munich, Garching, Germany
[d] Department of Diagnostic and Interventional Radiology, Technical University of Munich, School of Medicine and Klinikum rechts der Isar, Munich, Germany
[e] Chair of Biomedical Physics, Technical University of Munich, Garching, Germany
[f] Munich School of BioEngineering (MSB), Technical University of Munich, Garching, Germany
[g] Abteilung Analytische Pathologie, Helmholtz Zentrum München, Neuherberg, Germany
[h] TranslaTUM, Technical University of Munich, School of Medicine and Klinikum rechts der Isar, Munich, Germany
[i] Deutsches Konsortium für Translationale Krebsforschung (DKTK), Partner Site Munich, Munich, Germany

ARTICLE INFO

Keywords:
X-ray dark-field
CT scan
Radiation-induced lung damage
Preclinical study

ABSTRACT

Background and Purpose: Radiotherapy of thoracic tumours can lead to side effects in the lung, which may benefit from early diagnosis. We investigated the potential of X-ray dark-field computed tomography by a proof-of-principle murine study in a clinically relevant radiotherapeutic setting aiming at the detection of radiation-induced lung damage.
Material and Methods: Six mice were irradiated with 20 Gy to the entire right lung. Together with five unirradiated control mice, they were imaged using computed tomography with absorption and dark-field contrast before and 16 weeks post irradiation. Mean pixel values for the right and left lung were calculated for both contrasts, and the right-to-left-ratio R of these means was compared. Radiologists also assessed the tomograms acquired 16 weeks post irradiation. Sensitivity, specificity, inter- and intra-reader accuracy were evaluated.
Results: In absorption contrast the group-average of R showed no increase in the control group and increased by 7% ($p = 0.005$) in the irradiated group. In dark-field contrast, it increased by 2% in the control group and by 14% ($p = 0.005$) in the irradiated group. Specificity was 100% for both contrasts but sensitivity was almost four times higher using dark-field tomography. Two cases were missed by absorption tomography but were detected by dark-field tomography.
Conclusions: The applicability of X-ray dark-field computed tomography for the detection of radiation-induced lung damage was demonstrated in a pre-clinical mouse model. The presented results illustrate the differences between dark-field and absorption contrast and show that dark-field tomography could be advantageous in future clinical settings.

1. Introduction

Intrapulmonary tumours like lung cancer are frequently treated with radiotherapy. Radiotherapy of thoracic tumours is often associated with adverse effects for the lung because the absorbed dose can lead to inflammation, fibrosis or cancer [1]. In any case it is desirable to detect

* Corresponding author at: Dept. of Radiation Oncology, Klinikum rechts der Isar, TUM, Ismaninger Str. 22, 81675 München, Germany.
E-mail address: wilkens@tum.de (J.J. Wilkens).
[1] Contributed equally.

https://doi.org/10.1016/j.phro.2021.09.003
Received 3 December 2020; Received in revised form 13 September 2021; Accepted 13 September 2021
Available online 24 September 2021
2405-6316/© 2021 The Author(s). Published by Elsevier B.V. on behalf of European Society of Radiotherapy & Oncology. This is an open access article under the CC BY-NC-ND license (http://creativecommons.org/licenses/by-nc-nd/4.0/).

lung damage as early as possible so that treatment measures can be taken early on. Current clinical routine relies on absorption-based computed tomography (CT) for diagnostic purposes. The same holds true for preclinical small-animal research investigating emphysema [2–4], fibrosis [5–7] and radiotoxicity [8–10] in murine lungs. X-ray dark-field imaging [11] is an emerging technology, which can visualize information on the microscopic integrity of the alveolar structure of lung tissue [12–14]. It is by nature different from absorption-based imaging because it measures the small-angle scattering rather than the attenuation of X-rays. This makes dark-field imaging particularly suited for lung imaging, as this type of scattering appears on multiple microscopic air-tissue interfaces present there. Its application for the detection of lung disorders provided interesting results for inflammation [14], fibrosis [15–16], emphysema [17–20] and tumours [21]. Investigating its benefits for the detection of lung damages caused by radiotherapy has only started [16]. While these previous studies focussed on dark-field radiography, it is expected that dark-field tomography can provide enhanced image quality and additional information compared to radiography due to its three-dimensional nature without superimposed image features. However, the potential of X-ray dark-field tomography for the detection of radiation-induced lung damages has not yet been reported. To better understand the potential of X-ray dark-field CT for the detection of radiation-induced lung damage, we carried out a murine imaging study in a radiotherapeutic setting, with the hypothesis that dark-field CT is more sensitive than absorption CT to detect early stages of radiation-induced lung damage.

2. Materials and Methods

For this murine imaging study two small-animal research systems were used: the Small Animal Research Platform (SARRP, Xstrahl Ltd [22]) for image guided irradiation of the lung and a grating-based X-ray phase contrast and dark-field contrast prototype system (SkyScan 1190, Bruker microCT [23–25]) for tomographic imaging. The latter comprises a Talbot-Lau X-ray interferometer on a rotating gantry, including an X-ray tube, a source grating, a mouse bed, a phase grating, an analyser grating and a flat panel detector. The lung tomograms were evaluated quantitatively and assessed in a reader study.

2.1. Setups & irradiation

Image-guided irradiation of the right lung was performed at the SARRP with two opposing fields using 220 kVp X-rays filtered by 0.15 mm Copper at a dose rate of ~ 2 Gy / min. A planning cone beam CT (CBCT) with a voxel size of 0.25 × 0.25 × 0.25 mm^3 was taken on the SARRP with 60 kVp immediately before irradiation, and treatment planning based on this CBCT was done with the dedicated planning software MuriPlan (Xstrahl Ltd). An absorbed dose to water of 20 Gy was delivered to the entire right lung, which was defined on the planning CBCT. Further details can be found in Ref. [16]. The left lung was not irradiated and used as a reference for healthy tissue.

Tomographic imaging at the SkyScan setup was done with four phase steps (lateral movements of one grating) and 1.4 s exposure time per image at 37 kVp and 0.66 mA. A total of 211 projections distributed over 360° were acquired in a cone beam geometry. The total acquisition time per imaging session was 40 min, given by the exposure time for a single projection multiplied with the number of phase steps and the number of projections, plus overhead for gantry and grating movements. The imaging dose was well below 100 mGy [26]. Animals were anaesthetized intraperitoneally for stable positioning and were kept warm by a heating unit in the SkyScan setup. Remaining cardiac and breathing motion was not synchronized with the image acquisition, causing a certain degree of blur in the images. This means that smallest features could be blurred and difficult to classify. However, since our evaluation and in particular the reader study does not rely on smallest features, breathing motion is not considered as a limitation for our study. Processing of raw data and reconstruction of absorption and dark-field contrast images were performed with a statistical iterative reconstruction (SIR) algorithm [27], which uses a cost function to reduce noise in the reconstruction while maintaining sharp edges [25,27]. Reconstructed images had an isotropic voxel size of around 60 × 60 × 60 μm^3. The absorption contrast is based on the same physical principles as conventional clinical tomography, where the X-ray attenuation coefficient of the material is obtained, while the dark-field contrast is related to small-angle scattering of X-rays and a material specific "scattering coefficient" is shown in the images [11,23–24]. Tomograms were stored on a picture archiving and communication system (PACS) and assessed on a PACS workstation.

2.2. Animals & imaging study

The experiments were performed in accordance with the German law for animal protection. The animal study was approved by the District Government of Upper Bavaria with reference number 55.2-1-54-2532-77-2016. Female C57BL/6 mice (Charles River Laboratories) were chosen because they are sensitive to irradiation and to develop lung fibrosis [28]. Tomographic images were taken at the beginning of the study (before irradiation) and 16 weeks after irradiation. This point in time was selected because an earlier evaluation [16] showed that first manifestations of lung damage are detectable at this point in time, while the sensitivity of both contrast types is still expected to be below 100%. At the beginning, the experiment comprised a control group and an irradiated group of six mice each, but 16 weeks post irradiation one mouse of the control group is missing due to premature death. In total, 22 tomograms of both contrast types were obtained; 11 tomograms "before irradiation" and 11 tomograms "16 weeks post irradiation". As described in an earlier investigation [16], histopathological evaluation of formalin fixed and haematoxylin eosin stained tissue sections was performed 28 weeks post irradiation and showed a thickening of the alveolar walls in the affected area of the irradiated right lung, proving the presence of fibrosis. However, this does not mean that 16 weeks after irradiation (the time point used for the reader study) fibrosis was already present.

2.3. Quantitative analysis

The quantitative analysis was based on analysing average pixel values in three-dimensional lung segmentations in the tomograms. The segmentations covered the volumes of the left and right lung separately and were based on an automated lung segmentation in each tomogram that was further refined manually: The automated segmentation exploited both dark-field and absorption tomograms as well as geometric properties. Dark-field tomograms show primarily scattering material such as the lung, so the lung contributions dominate their histograms. Adding that the lungs are found in the central region of the tomogram, a combination of prefiltering, thresholding and calculations of the center of mass was used to get a suitable estimate for a mask of the lung. This mask usually overshoots the actual lung region a bit and thus contains also bones and non-lung tissue. By applying this mask to the absorption-based tomograms and another thresholding step, the lung mask was further refined. A k-means algorithm was employed to separate the lung into two parts. Finally, this mask was inspected visually and refined manually (if necessary) using standard segmentation tools. Because of the way the raw data is acquired, absorption and dark-field tomograms are intrinsically co-registered. Thus, quantitative analysis covers the exact same regions in the specimen for both contrasts. For the left and right lung, mean pixel values m_{right} and m_{left} were determined. The ratio $R = m_{right}/m_{left}$ was calculated to quantify the average absorption and average scattering normalized to healthy lung tissue for an investigated image. The group-average values of R at both points in time (before and 16 weeks after irradiation) were used for statistical testing. Corresponding p-values were calculated relative to the same group but between both points in time with a two-sided Mann-Whitney U Test

(performed with Python SciPy v1.6.2).

2.4. Reader study

All tomograms acquired 16 weeks after irradiation were assessed by three radiologists (APS, FM, AAF) having 4, 2 and 9 years of experience with X-ray dark-field imaging in (pre-)clinical research. The radiologists were aware that some of the mice had received lung irradiation. They assessed both lungs separately and were asked to classify them as either healthy or damaged. In this study design, sensitivity and specificity are represented by two conditions:

Sensitivity: only the right lung was classified as damaged for an irradiated mouse.
Specificity: both lungs were classified as healthy for an unirradiated mouse.

Further, inter-reader and intra-reader agreement and accuracy were determined. Here 'agreement' solely refers to the readers coming to the same assessment regardless of whether the mouse was irradiated or not. The 'accuracy' then also attributes for the fact that the mouse was either irradiated or not. The differentiation between agreement and accuracy is made here to emphasize that readers can come to the same assessment based on the tomograms but that that assessment does not necessarily reflect the real situation.

3. Results

3.1. Quantitative analysis

For the control group, the group-average value of R did not change between before irradiation and 16 weeks after irradiation (mean 0%, Min/Max: [−3.3%, 3.0%]) in absorption tomograms and increased by less than 2% (Min/Max: [−0.6%, 3.1%]) in dark-field tomograms (Fig. 1). For the irradiated group, the group-average value of R increased by about 7% (Min/Max: [2.5%, 14%], $p = 0.005$) in absorption tomograms and decreased by about 14% (Min/Max: [5%, 25%], $p = 0.005$) in dark-field tomograms (Fig. 1).

3.2. Reader study

In none of the assessed tomograms the readers detected any damage in the left (not irradiated, healthy) lung. Thus, deviations of sensitivity and specificity from the ideal case are solely caused by the assessment of the right lung. In the following, detailed results of the reader study will be presented for absorption tomography first, followed by dark-field tomography and finally their comparison. The numerical values for sensitivity, specificity and accuracy are summarized in Tables 1 and 2.

For absorption tomography, the readers showed an average sensitivity of 19% (Min/Max: [0%, 33%]) and an average specificity of 93% (Min/Max: [80%, 100%]). The false classification of healthy lungs can be attributed to a single reader (first reader in Table 1, Fig. 2) who observed abnormal lung tissue in the right lung of one of the healthy mice. However, this reader also pointed out that this abnormality was not caused by irradiation. Thus, considering the definition of the specificity above, one could claim that the specificity is actually 100%, which was used for subsequent calculations. The average inter-reader agreement was 88% (Min/Max: [82%, 100%]). All readers agreed entirely on four of the six irradiated mice but classified all of them as healthy. Further, in no case all readers agreed on the lung being damaged. Therefore, the average inter-reader accuracy for absorption tomography was 45% for three readers. The average intra-reader agreement was 97% (Min/Max: [90%, 100%]) because there was only one case in which a reader changed his opinion in the second read. The average intra-reader accuracy was 58% and the average accuracy was 59% (Min/Max: [36%, 64%]).

For dark-field tomography, the readers showed an average sensitivity of 75% (Min/Max: [67%, 83%]) and an average specificity of 100%. The healthy mouse that was classified as damaged (but not induced by irradiation) in absorption tomography was classified as healthy in dark-field tomography (Fig. 2). The average inter-reader agreement was 92% (Min/Max: [90%, 100%]). All the readers agreed entirely on four of the six irradiated mice in dark-field classifying the right lung in each case as damaged. In one case the readers agreed entirely on the lung being healthy although it was irradiated. In another case there was partial agreement between readers. Thus, the average inter-reader accuracy was 82% for three readers. The average intra-reader agreement was 97% (Min/Max: [90%, 100%]) because there was also one case in which the reader changed his opinion in the second read (not the same mouse as in absorption tomography). The average intra-reader accuracy was 85% and the average accuracy was 86% (Min/Max: [82%, 90%]).

In comparison, the average accuracy was 45% higher for dark-field contrast compared to absorption contrast. Intra-reader and inter-

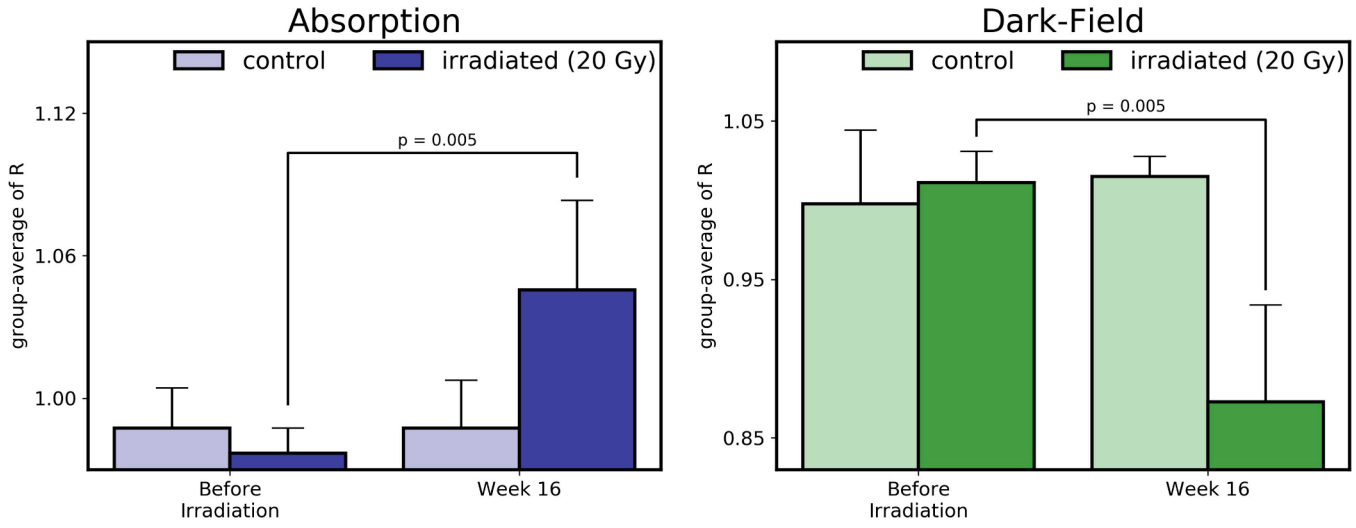

Fig. 1. Results of the quantitative analysis of the group-average value of R for absorption (left) and dark-field (right). Left: In absorption, the group average for the control group shows no significant change but the group average for the irradiated group increased significantly. Right: In dark-field, the group average for the control group increased slightly but not significantly. The group average for the irradiated group decreased significantly.

Table 1
Sensitivity and specificity for absorption (A) and dark-field (DF) tomograms. Tabulated are the results from the first and second read for each reader. *: Note that for further evaluation a specificity of 100% for absorption tomograms assessed by the first reader was used (see section 3.2).

	Sensitivity						Specificity					
	1st Reader		2nd Reader		3rd Reader		1st Reader		2nd Reader		3rd Reader	
	1st Read	2nd Read	1st Read	2nd Read	1st Read	2nd Read	1st Read	2nd Read	1st Read	2nd Read	1st Read	2nd Read
A	16.7% (1/6)	33.3% (2/6)	0.0%	0.0%	33.3% (2/6)	33.3% (2/6)	80.0%* (4/5)	80.0%* (4/5)	100%	100%	100%	100%
DF	66.7% (4/6)	83.3% (5/6)	83.3% (5/6)	83.3% (5/6)	66.7% (4/6)	66.7% (4/6)	100%	100%	100%	100%	100%	100%

Table 2
Accuracy for absorption and dark-field tomography obtained from the results of the reader study.

	Absorption Contrast				Dark-Field Contrast			
	1st Reader	2nd Reader	3rd Reader	Inter-Reader	1st Reader	2nd Reader	3rd Reader	Inter-Reader
1st Read	63.6%	45.4%	63.6%	45.4%	81.8%	90.1%	81.8%	81.8%
2nd Read	72.7%	45.4%	63.6%	45.4%	90.1%	90.1%	81.8%	81.8%
Intra-Reader	63.6%	45.4%	63.6%	x	81.8%	90.1%	81.8%	x

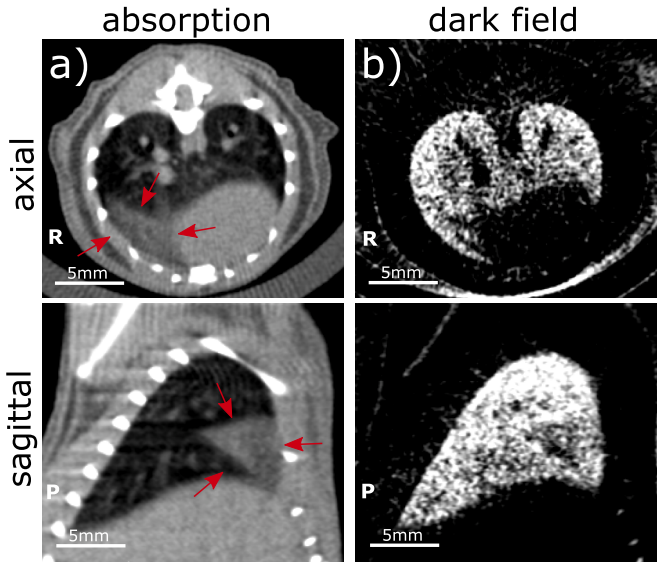

Fig. 2. Axial (top row) and sagittal (bottom row) slices of the one mouse that was not irradiated but whose lung was classified as damaged in absorption tomography (a) while it was classified as healthy in dark-field tomography (b). Slices show the exact same location in tomograms of both contrasts. In a) the region of the abnormal tissue is marked with red arrows. In dark-field contrast b) this region shows lower contrast but the angled area is still visible. Note that the reader pointed out that this abnormal tissue is not caused by irradiation.

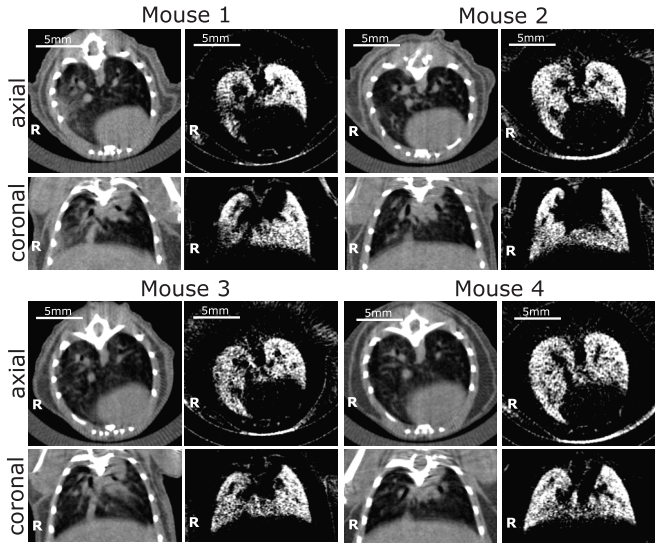

Fig. 3. Axial (first and third row) and coronal (second and fourth row) slices of absorption (first and third column) and dark-field (second and fourth) tomograms from four different mice of the irradiated group (20 Gy) acquired 16 weeks post irradiation. Mouse 1 shows the highest agreement rate in absorption tomography (damage visible on the right lateral side in both contrasts). Mouse 2 and 3 are the ones that were constantly missed in absorption tomography but found in dark-field tomography (damage visible throughout the right lung). Especially in Mouse 3 the difference between absorption and dark-field signal of the right lung is visible. Mouse 4 is the one that was missed in both contrasts.

reader accuracy were higher in dark-field than in absorption. The sensitivity was two to four times higher for dark-field tomography in comparison to absorption tomography (on average almost four times higher; see Table 1). Two irradiated cases that were missed by all readers using absorption tomography were always detected with dark-field tomography (Mouse 2 and 3 in Fig. 3). One case was missed entirely in both contrasts. For all other cases there was partial agreement between the two contrasts. The case of the healthy mouse that was assessed to have lung damage absorption tomography but was classified as healthy in dark-field tomography is shown in Fig. 2. It illustrates the different nature of the absorption and dark-field signal showing a noticeable deviation from healthy tissue in absorption tomography (red arrows) that is less visible in dark-field tomography.

4. Discussion

We conducted a proof-of-principle study for the detection of radiation-induced lung damage using X-ray dark-field CT and absorption-based CT. Two groups of mice were investigated, a control group and a group that received irradiation (20 Gy) to the entire right lung, with imaging performed before irradiation and 16 weeks post irradiation. For both groups mean pixel values of irradiated and healthy lung tissue were calculated. Dark-field contrast showed an average decrease of 14% ($p = 0.005$) from healthy tissue while for absorption there was an average increase of 7% ($p = 0.005$). The decrease of the dark-field signal is caused by the reduction of air-tissue interfaces, which reduces the small-angle scattering of X-rays [12,17,21], while the

increase in absorption is caused by consolidation of lung tissue. Note that these two phenomena are interrelated. Additionally, the performance of X-ray dark-field tomography was compared to that of absorption-based tomography in a reader study. The specificity was 100% in both contrasts but the average sensitivity was almost four times higher using dark-field. Both contrasts showed consistent intra-reader agreement with only one reader changing his opinion in the second read. Additionally, readers were more likely to consistently agree among each other using dark-field tomography in comparison to absorption-based tomography. Furthermore, we observed two cases that would not have been detected by any of the three readers using absorption-based tomography but were rated consistently by all readers using dark-field tomography. Thus, sensitivity as well as inter-reader and intra-reader accuracy were higher for dark-field tomography. Altogether, dark-field tomography showed a higher accuracy for the detection of radiation-induced lung damage than absorption-based tomography.

However, in one case absorption-based tomography provided images of an altered state of the lung in a control mouse which was less visible by dark-field tomography. Since this mouse was not irradiated and since it was pointed out by one of the readers that this alteration is usually not caused by irradiation, this case was considered as a correct classification. Nonetheless, the presented cases show that dark-field tomography provides complementary information to absorption-based tomography as the former provides a high sensitivity for changes of the alveolar structure while the latter allows an additional assessment of surrounding tissues. Previous studies related the additional information in the dark-field signal to small-angle scattering by lung tissue which is influenced by the state of the lung [12–21]. Also, presently, radiologists are better trained in absorption-based imaging. Therefore, absorption-based tomography can serve as a reference for training radiologists in dark-field imaging.

One has to note that our study did not include a histological confirmation of the biological state of the lung at the point in time of image acquisition (16 weeks post irradiation), although fibrosis was confirmed histologically at a later point in time (28 weeks post irradiation). However, based on earlier investigations and the comparison with the control group, we can assume with a very high likelihood that the apparent changes seen in lung images are indeed indications for radiation-induced lung damage. As a follow up to the current study, investigations with larger animal cohorts are required in which mice can be sacrificed at different points in time in order to resolve the exact state of their lung histology over time and to match histological data with absorption and dark-field signals. Image quality is limited by dose and by the time animals can be kept in anaesthesia, therefore a protocol with a maximum of 211 projections over 40 min had to be chosen.

Previous dark-field imaging studies used mainly radiographic imaging data and found higher sensitivity when using dark-field radiography. The field still lacks comparison between absorption-based tomography and dark-field tomography for a variety of diseases that were already investigated with radiographic imaging [12–21]. Generally, tomographic studies of any contrast type can be expected to be more sensitive than the respective radiographs. Compared to our radiographic imaging study covering radiation-induced lung damages [16] we found higher sensitivity and specificity for both contrasts accompanied by less inconsistencies among readers, at a relatively early point in time where changes in lung tissue just started to become visible in imaging. The higher dose of tomographic dark-field imaging compared to dark-field radiography could then be justified to detect early stages of lung damage which would still be hidden in radiographs. An example of this early detection are the two mice presented here in which all readers agreed that the lung was healthy based on absorption CT, but they also all agreed that the same lung was not healthy based on dark-field CT – an observation that was much more pronounced here in CT than in our studies using radiographic imaging [16].

Comparing our study to dark-field radiography studies that focused on other diseases is challenging due to differences in methodology. Nonetheless in each of the previous studies dark-field provided higher or equal sensitivity compared to absorption-based imaging which is what we could confirm in our study. However, all of the above studies were carried out with murine specimen and it is yet to be determined how these results translate to humans. First steps have been undertaken in that direction [29].

In conclusion, our results underline the observation that absorption and dark-field imaging provide distinct information about the state of lung tissue. Additionally, it was shown that dark-field tomography is capable to provide a higher sensitivity than absorption-based tomography for the detection of radiation-induced lung damage.

Acknowledgments

We acknowledge financial support through the DFG (Gottfried Wilhelm Leibniz program) and the European Research Council (AdG 695045). This work was carried out with the support of the Karlsruhe Nano Micro Facility (KNMF, www.kit.edu/knmf), a Helmholtz Research Infrastructure at Karlsruhe Institute of Technology (KIT).

Declaration of Competing Interest

The authors declare that they have no known competing financial interests or personal relationships that could have appeared to influence the work reported in this paper.

References

[1] Coggle JE, Lambert BE, Moores SR. Radiation effects in the lung. Environ Health Perspect 1986;70:261–91.
[2] Postnov AA, Meurrens K, Weiler H, Van Dyck D, Xu H, Terpstra P, et al. In vivo assessment of emphysema in mice by high resolution X-ray microtomography. J Microsc 2005;220:70–5.
[3] Froese AR, Ask K, Labiris R, Farncombe T, Warburton D, Inman MD, et al. Three-dimensional computed tomography imaging in an animal model of emphysema. Eur Respir J 2007;30:1082–9.
[4] Artaechevarria X, Blanco D, de Biurrun G, Ceresa M, Pérez-Martín D, Bastarrika G, et al. Evaluation of micro-CT for emphysema assessment in mice: Comparison with non-radiological techniques. Eur Radiol 2011;21:954–62.
[5] Saito S, Murase K, Muñoz-Barrutia A. Detection and early phase assessment of radiation-induced lung injury in mice using micro-CT. PLoS ONE 2012;7:e45960.
[6] Perez JR, Lee S, Ybarra N, Maria O, Serban M, Jeyaseelan K, et al. A comparative analysis of longitudinal computed tomography and histopathology for evaluating the potential of mesenchymal stem cells in mitigating radiation-induced pulmonary fibrosis. Sci Rep 2017;7:9056.
[7] De Langhe E, Vande Velde G, Hostens J, Himmelreich U, Nemery B, Luyten FP, et al. Quantification of lung fibrosis and emphysema in mice using automated micro-computed tomography. PLoS ONE 2012;7:e43123.
[8] Vande Velde G, De Langhe E, Poelmans J, Bruyndonckx P, d'Agostino E, Verbeken E, et al. Longitudinal in vivo microcomputed tomography of mouse lungs: No evidence for radiotoxicity. Am J Physiol Lung Cell Mol Physiol 2015;309:L271–9.
[9] Detombe SA, Dunmore-Buyze J, Petrov IE, Drangova M. X-ray dose delivered during a longitudinal micro-CT study has no adverse effect on cardiac and pulmonary tissue in C57BL/6 mice. Acta Radiol 2013;54:435–41.
[10] Granton PV, Dubois L, van Elmpt W, van Hoof SJ, Lieuwes NG, De Ruysscher D, et al. A longitudinal evaluation of partial lung irradiation in mice by using a dedicated image-guided small animal irradiator. Int J Radiat Oncol Biol Phys 2014;90:696–704.
[11] Pfeiffer F, Bech M, Bunk O, Kraft P, Eikenberry EF, Brönnimann Ch, et al. Hard-X-ray dark-field imaging using a grating interferometer. Nature Mater 2008;7:134–7.
[12] Schleede S, Meinel FG, Bech M, Herzen J, Achterhold K, Potdevin G, et al. Emphysema diagnosis using X-ray dark-field imaging at a laser-driven compact synchrotron light source. Proc Natl Acad Sci USA 2012;109:17880–5.
[13] Meinel FG, Schwab F, Schleede S, Bech M, Herzen J, Achterhold K, et al. Diagnosing and mapping pulmonary emphysema on X-Ray projection images: incremental value of grating-based X-ray dark-field imaging. PLoS ONE 2013;8:e59526.
[14] Hellbach K, Meinel FG, Conlon TM, Willer K, Yaroshenko A, Velroyen A, et al. X-ray dark-field imaging to depict acute lung inflammation in mice. Sci Rep 2018;8:2096.
[15] Yaroshenko A, Hellbach K, Yildirim AÖ, Conlon TM, Fernandez IE, Bech M, et al. Improved in vivo assessment of pulmonary fibrosis in mice using X-ray dark-field radiography. Sci Rep 2015;5:17492.
[16] Burkhardt R, Gora T, Fingerle AA, Sauter AP, Meurer F, Umkehrer S, et al. Early detection of radiation-induced lung damage with X-ray dark-field radiography in mice. Eur Radiol 2021;31:4175–83.

[17] Yaroshenko A, Hellbach K, Bech M, Grandl S, Reiser MF, Pfeiffer F, et al. Grating-based X-ray dark-field imaging: a new paradigm in radiography. Curr Radiol Rep 2014;2:57.
[18] Meinel FG, Yaroshenko A, Hellbach K, Bech M, Müller M, Velroyen A, et al. Improved diagnosis of pulmonary emphysema using in vivo dark-field radiography. Invest Radiol 2014;49:653–8.
[19] Hellbach K, Yaroshenko A, Meinel FG, Yildirim AÖ, Conlon TM, Bech M, et al. In vivo dark-field radiography for early diagnosis and staging of pulmonary emphysema. Invest Radiol. 2015;50:430–5.
[20] Yaroshenko A, Meinel FG, Bech M, Tapfer A, Velroyen A, Schleede S, et al. Pulmonary emphysema diagnosis with a preclinical small-animal X-ray dark-field scatter-contrast scanner. Radiology 2013;269:427–33.
[21] Scherer K, Yaroshenko A, Bölükbas DA, Gromann LB, Hellbach K, Meinel FG, et al. X-ray dark-field radiography - in-vivo diagnosis of lung cancer in mice. Sci Rep 2017;7:402.
[22] Wong J, Armour E, Kazanzides P, Iordachita I, Tryggestad E, Deng H, et al. High-resolution, small animal radiation research platform with X-ray tomographic guidance capabilities. Int J Radiat Oncol Biol Phys 2008;71:1591–9.
[23] Bech M, Tapfer A, Velroyen A, Yaroshenko A, Pauwels B, Hostens J, et al. In-vivo dark-field and phase-contrast X-ray imaging. Sci Rep 2013;3:3209.
[24] Tapfer A, Bech M, Velroyen A, Meiser J, Mohr J, Walter M, et al. Experimental results from a preclinical X-ray phase-contrast CT scanner. Proc Natl Acad Sci USA 2012;109:15691–6.
[25] Velroyen A, Yaroshenko A, Hahn D, Fehringer A, Tapfer A, Müller M, et al. Grating-based X-ray dark-field computed tomography of living mice. EBioMedicine 2015;2:1500–6.
[26] Umkehrer S, Birnbacher L, Burkhardt R, von Teuffenbach M, Yildirim AÖ, Pfeiffer D, et al. Optimization of in vivo murine X-ray dark field computed tomography. Rev Sci Instrum 2019;90:103103.
[27] Hahn D, Thibault P, Fehringer A, Bech M, Koehler T, Pfeiffer F, et al. Statistical iterative reconstruction algorithm for X-ray phase-contrast CT. Sci Rep 2015;5:10452.
[28] Walkin L, Herrick SE, Summers A, Brenchley PE, Hoff CM, Korstanje R, et al. The role of mouse strain differences in the susceptibility to fibrosis: A systematic review. Fibrogenesis Tissue Repair 2013;6:18.
[29] Fingerle AA, De Marco F, Andrejewski J, Willer K, Gromann LB, Noichl W, et al. Imaging features in post-mortem X-ray dark-field chest radiographs and correlation with conventional x-ray and CT. Eur Radiol Exp 2019;3:25.